ARTICLE

J. Cent. South Univ. (2019) 26: 1521−1529
DOI: https://doi.org/10.1007/s11771-019-4108-5

Springer

Na_2FePO_4F/C composite synthesized via a simple solid state route for lithium-ion batteries

HU Hai(胡海)[1, 2], WANG Yu(王誉)[1, 2], HUANG Yan(黄妍)[1, 2],
SHU Hong-bo(舒洪波)[1, 2], WANG Xian-you(王先友)[1, 2]

1. School of Mechanical Engineering and School of Chemistry, Xiangtan University, Xiangtan 411105, China;
2. National Base for International Science & Technology Cooperation, National Local Joint Engineering Laboratory for Key Materials of New Energy Storage Battery, Hunan Province Key Laboratory of Electrochemical Energy Storage and Conversion, Xiangtan 411105, China

Abstract: Using low-cost $FePO_4·2H_2O$ as iron source, Na_2FePO_4F/C composite is prepared by alcohol-assisted ball milling and solid-state reaction method. The XRD pattern of Na_2FePO_4F/C composite demonstrates sharp peaks, indicating high crystalline and phase purity. The SEM and TEM images reveal that diameter of the spherical-like Na_2FePO_4F/C particles ranges from 50 to 300 nm, and HRTEM image shows that the surface of Na_2FePO_4F/C composite is uniformly coated by carbon layer with a average thickness of about 3.6 nm. The carbon coating constrains the growth of the particles and effectively reduces the agglomeration of nanoparticles. Using lithium metal as anode, the composite delivers a discharge capacities of 102.8, 96.4 and 90.3 mA·h/g at rates of 0.5*C*, 1*C* and 2*C*, respectively. After 100 cycles at 0.5*C*, a discharge capacity of 98.9 mA·h/g is maintained with capacity retention of 96.2%. The Li^+ diffusion coefficient (*D*) of Na_2FePO_4F/C composite is calculated as 1.71×10^{-9} cm^2/s. This study reveals that the simple solid state reaction could be a practical and effective synthetic route for the industrial production of Na_2FePO_4F/C material.

Key words: lithium-ion batteries; Na_2FePO_4F/C composite; alcohol-assisted ball milling; solid state reaction; spherical-like particles

Cite this article as: HU Hai, WANG Yu, HUANG Yan, SHU Hong-bo, WANG Xian-you. Na_2FePO_4F/C composite synthesized via a simple solid state route for lithium-ion batteries [J]. Journal of Central South University, 2019, 26(6): 1521−1529. DOI: https://doi.org/10.1007/s11771-019-4108-5.

1 Introduction

For several decades, LIBs have been investigated and utilized in energy storage system and portable electronic devices due to the outstanding electrochemical performance [1–4]. So far, the advanced cathode materials become the key issues for development of high performance LIBs. At present, commercial cathode materials including $LiCoO_2$, $LiMn_2O_4$ and $LiFePO_4$ [5–8] have been applied to electronic device. $LiFePO_4$ has been considered a promising material owing to its non-toxic, abundant resource and safety. However, the demand for lithium is increasing in the recent years due to rapid growth of electric vehicle and

Foundation item: Projects(51472211, 51502256) supported by the National Natural Science Foundation of China; Projects(2016GK4005, 2016GK4030) supported by the Strategic New Industry of Hunan Province, China; Project(13C925) supported by the Research Foundation of Education Bureau of Hunan Province, China
Received date: 2018-09-30; **Accepted date:** 2019-03-07
Corresponding author: WANG Xian-you, PhD, Professor; Tel: +86-731-58293377; E-mail: wxianyou@yahoo.com; ORCID: 0000-0001-8888-6405

mobile electronic devices, thus lithium resource diminishes quickly. In contrast to lithium, sodium resource is abundant and sodium's radius is closer to lithium within alkali metal [9–13]. Therefore, sodium and iron-based materials have attracted more attention as promising candidates for cell cathode. For instance, $NaFeO_2$ [14], $NaFeF_3$ [15] and $NaFePO_4$ [16] have been used as cathode material. Among these materials, Na_2FePO_4F stands out due to its special two-dimensional channels structure and small volume change (3.7%) on the electrochemical reaction [17].

Na_2FePO_4F was firstly reported by ELLIS et al [18], and then further investigated by researchers for LIBs [17, 19−22]. Such phosphate presents high working voltage (3.6 V vs. Li/Li^+) and considerable safety advantage because of the induction of PO_4^{3-} and the strong electro-negativity of F^- [23]. In LIBs system, the reaction mechanism of Na_2FePO_4F cathode can be explained by a Li/Na exchange [24, 25]. Na^+ extraction from and Li^+ insertion in the lattice occurs during the first few cycling process, namely the Na^+ site is replaced by Li^+ in Na_2FePO_4F crystallographic. The $NaFePO_4F$ intermediate phase exhibits a volume expansion of unit cell compared to $LiFePO_4F$, thus facilitating the insertion/extraction of Li^+. The chemical reaction equations is described as follows: $Na_2FePO_4F \rightarrow NaFePO_4F+Na^++e$, and then: $NaFePO_4F+Li^++e \rightarrow (Li, Na)FePO_4F$. Meanwhile, Li^+ insertion/extraction occurs at the graphite counter electrode. Even in the presence of Na^+, the graphite anode is electrochemically inactive in the electrolyte. Therefore, it may be promising that Na_2FePO_4F is utilized as cathode of LIBs for electric vehicle and energy storage devices.

As one of phosphates, electrical conductivity of Na_2FePO_4F is relative low, which leads to low specific capacity, unsatisfying cycling life and rate capability. As known to all, carbon coating is an effective way to enhance the electrical conductivity. In most cases, carbon sources such as citric acid [20], acetylene black [22], and ascorbic acid [26], are applied to improve the electrical conductivity of Na_2FePO_4F. Reported synthesis methods are solid-state reaction [18, 22], sol-gel [20], ion thermal [17], hydrothermal [19], and spray-drying methods [27]. Among these methods, solid state method is usually adopted in practical because of easy operation and simple synthetic procedure. But there are some disadvantages including non-uniform carbon coating and serious agglomeration. To solve the problem, a modified method, by which reactants are mixed by ball milling in alcohol and calcinated at high temperature, is put forward to synthesize Na_2FePO_4F/C composite. The as-prepared composite is composed of nanoparticles (50–300 nm), the surface of which is uniformly coated by thin carbon layer, and a small amount of particles come together. The structure, morphology and electrochemical performance of Na_2FePO_4F/C composite are studied in detail.

2 Experimental

2.1 Material synthesis

Na_2FePO_4F/C composite was synthesized by a modified solid state reaction from stoichiometric amounts of $FePO_4·2H_2O$, $NaHCO_3$, NaF and glucose. The precursors were mixed by ball milling for 3 h in alcohol. The mixture was dried at 70 °C for 12 h. The obtained powder was pre-sintered at 350 °C for 3 h, and further sintered at 600 °C for 8 h under Ar.

2.2 Material characterizations

The crystal structure of Na_2FePO_4F/C composite was tested over 2θ interval of 10°–80° by Rigaku D/MAX-2500 X-ray diffraction using Cu K_a radiation (λ=1.54178 Å) and a graphite monochromator with a scan rate of 5°/min. The morphologies and microstructure were analyzed by using a JEOL JSM-6610 scanning electron morphologe (SEM) and JEM-2100F transmission electron microscope (TEM). Energy-dispersive X-ray spectroscopy (EDX) was performed on the TEM system with an EDX attachment. Raman spectra were collected using Macro-Raman spectrometer (Renishaw invia Raman microscope). Elemental analysis on carbon was performed by Vario EL III elemental analyzer. The specific surface area was determined using the Brunnauer-Emmett-Teller (BET) surface adsorption method (BET micromeritics tristar 3000).

2.3 Electrochemical measurements

Coin-type cells (2025 type) were made in the argon-filled glove box, where oxygen and moisture concentrations were both less than 5×10^{-6}. The

electrode was composed of 70% cathode material, 20% acetylene black, and 10% polyvinylidene fluoride (PVDF) binder. The mass of the positive active material is about 3.57 mg/cm^2 per electrode. The testing cells were composed of as-prepared cathode, lithium foil negative electrode, Celgard 2300 separator, and 1 mol/L $LiPF_6$/(V(EC): V(DMC)=1:1) as the electrolyte. Electrochemical tests were performed at 25 °C under 2.0–4.5 V utilizing the galvanostatic charge/discharge unit of NetWare battery system BTS-XWJ-6.44S-00052. Specific capacity was calculated based on the mass of active materials. Cyclic voltammetry (CV) experiments were carried out at different scan rates using a VersaSTAT3 electrochemical workstation (Princeton, America). EIS was also performed on a VersaSTAT3 electrochemical workstation.

3 Results and discussion

3.1 Materials characterizations

Figure 1(a) displays the XRD pattern of Na_2FePO_4F/C composite. The XRD pattern of Na_2FePO_4F/C matches well with the standard pattern (ICSD No: 167044) of the orthorhombic structure with the Pbcn space group [18]. The single phase Na_2FePO_4F is similar to the structure of $Na_2FePO_4(OH)$ [28], analogous to Na_2MgPO_4F [29] and Na_2CoPO_4F [30]. No impurity peaks are detected, indicating high phase purity. Moreover, carbon peaks are not observed in the diffraction pattern of sample, implying amorphous state of carbon. Figure 1(b) displays the crystal structure model of Na_2FePO_4F. Apparently, dioctahedral $Fe_2O_7F_2$ units, composed of sharing-face FeO_4F_2 octahedra, are connected with F atoms to construct chains. These chains are linked by PO_4 to form [$FePO_4F$] layers which provide two-dimensional channels for ion movement [18, 19, 31, 32].

The SEM image (Figure 2(a)) reveals that the size of Na_2FePO_4F particles is in the range of 50–300 nm. The particles are homogeneous-dispersed, and few particles conglomeration is found between nearby particles. The TEM image (Figure 2(b)) confirms that spherical-like Na_2FePO_4F/C composite is composed of small primary nanoparticles. Further investigation into Na_2FePO_4F/C composite is performed using HRTEM as shown in Figure 2(c), and the fast Fourier transform (FFT) graph is displayed in the inset of Figure 2(c). Clear lattice fringes are observed from Figure 2(c), reflecting that Na_2FePO_4F/C sample is well crystalline. The crystal fringes with a spacing of about 0.393 nm associated with (121) plane of Na_2FePO_4F (d_{121}= 3.933 Å). Moreover, the outer of nanoparticles is uniformly encapsulated by carbon layer of about 3.6 nm thickness, by which small particles connect to form excellent conductive network. The signals of Na, Fe, P, O and F can be determined in Figure 2(d), and the Cu peaks come from a copper collector. The atomic mole ratios are obtained by EDX result, x(Na) : x(Fe) : x(P) : x(F)=10.97 : 5.26 : 5.43 : 5.38, which is near to the theoretical value of 2 : 1 : 1 : 1. The carbon fraction in Na_2FePO_4F/C is determined to be 2.35% by carbon & sulfur analyzer.

Raman spectrum is applied to analyzing carbon species on Na_2FePO_4F/C composite (Figure 3(a)). The strong D and G peaks are

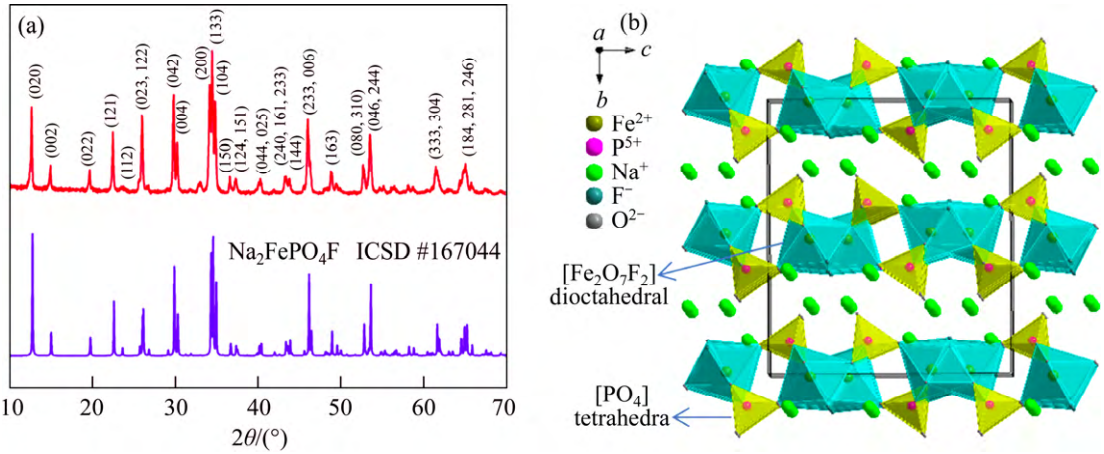

Figure 1 XRD pattern of Na_2FePO_4F/C composite (a) and crystal structure of Na_2FePO_4F with space group Pbcn, viewed along [100] (b)

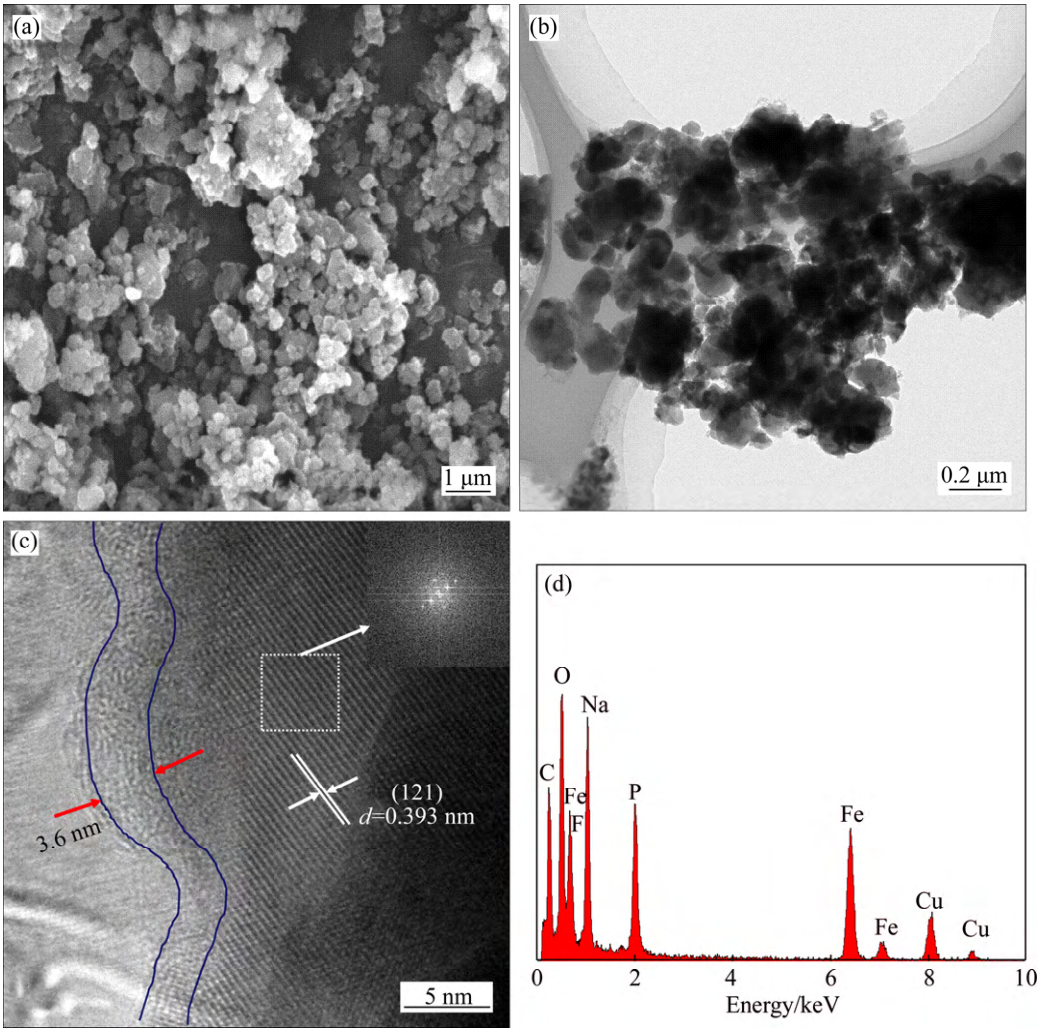

Figure 2 SEM image (a), TEM (b) and HRTEM (c) images and energy-dispersive X-ray spectrum (d) of Na_2FePO_4F/C composite

observed at 1348 and 1587 cm^{-1}, respectively. Generally, the G-band is attributed to graphitic carbon, and the D-band is related to disorder carbon. I_D/I_G is usually used to identify the degree of carbon disorder. The calculated I_D/I_G is 0.89, which is bigger than that of using mixed carbon source [33]. The result shows disorder carbon is the major component of carbon layer. Additionally, it is noted that Raman scatting by PO_4^{3-} in the range of 300–1100 cm^{-1} is not observed and the Raman signals of carbon are mainly found with G and D bands. The analyses further confirm the purity phase of Na_2FePO_4F, which is consistent with XRD result. The N_2 adsorption–desorption of Na_2FePO_4F/C is displayed in Figure 3(b). The isotherm with a hysteresis loop appeared at high pressure (p/p_o>0.8) belongs to a typical of IV isotherm. A surface area value of 24.7 m^2/g is calculated by means of BET method.

3.2 Electrochemical properties

The as-prepared samples have been tested in lithium-ion batteries. Figure 4 shows charge/discharge curves of Na_2FePO_4F/C in the first five cycles at 0.1*C* (12.4 mA/g). The initial charge/discharge capacity are 109.2 and 120.9 mA·h/g, respectively, and the columbic efficiency is 110.7%. The high columbic efficiency is probably because of the excessive amount of ions (Li^+/Na^+) insert into vacancies (Na site) of the Na_2FePO_4F/C crystal compared with the charge process, similar results have been reported by ELLIS et al [18]. The two obvious charge platforms and the two discharge platforms appear at 3.0 and 3.7, 2.9 and 3.6 V, respectively. After three cycles, the ion-exchange has completed and $NaLiFePO_4F$ phase is formed [19, 22]. The curve shows a repetitive loop of charging and discharging, and the reversible

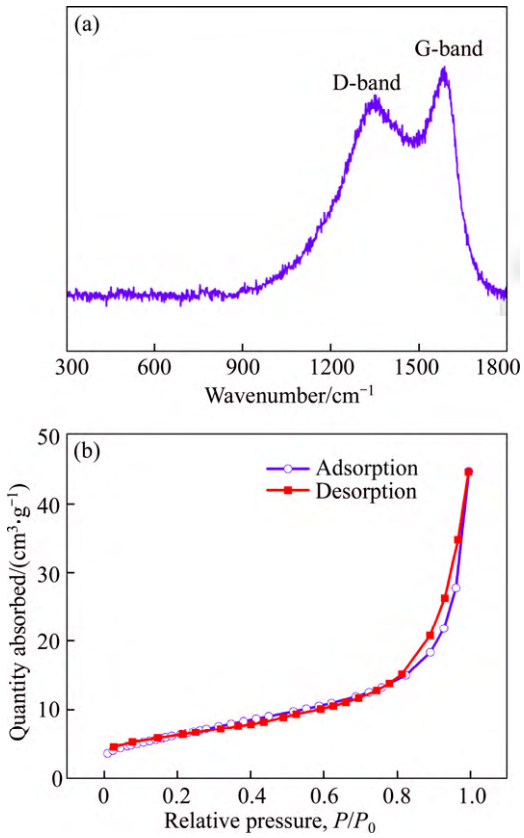

Figure 3 Raman spectrum (a) and N_2 adsorption-desorption isotherm (b) of Na_2FePO_4F/C composite

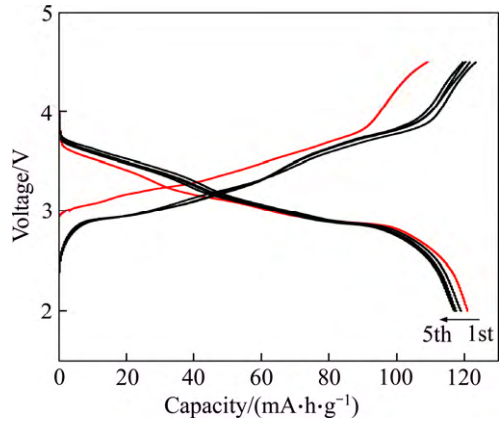

Figure 4 Charge/discharge curves of Na_2FePO_4F/C composite at 0.1*C*

discharge capacity of 117.8 mA·h/g can be retained.

The charge/discharge curves of Na_2FePO_4F/C composite at the various rates are displayed in Figure 5(a). The discharge capacities gradually decrease with increasing discharge current density, meanwhile, the electrode polarization increases. Figure 5(b) shows the rate capability with a sustain discharge capacity of 118.5, 102.8, 96.4, 90.3 and 55.7 mA·h/g at 0.1*C*, 0.5*C*, 1*C*, 2*C* and 5*C*, respectively. When the current density is reduced back to 0.1*C*, the capacity is almost equal to the original value (118.5 mA·h/g). The rate performance in our work is superior to the recently reported works. For example, CUI et al [33] synthesized Na_2FePO_4F/C by a carbothermal reduction, and the electrode exhibited discharge capacity of 74 mA·h/g at 1*C* and 52 mA·h/g at 2*C*. BRISBOIS et al [34] prepared Na_2FePO_4F/C microsphere using spray-drying method, and a discharge capacity of 78 mA·h/g at 1*C* rate was achieved. Figure 5(c) displays the cycling performance of the Na_2FePO_4F/C composite at 0.5*C*. An initial discharge capacity of 102.8 mA·h/g is delivered and 98.9 mA·h/g is maintained after 100 cycles with capacity retention of 96.2%. The Na_2FePO_4F/C cathode reported by CUI et al [33] delivered a capacity of 110 mA·h/g at 0.1*C*, and only 91% of capacity could be retained after 30 cycles. Apparently, the Na_2FePO_4F/C composite in our work exhibits better cycling performance.

Figure 6(a) shows CV curves of Na_2FePO_4F/C composite at different scan rates of 0.1 to 1 mV/s. As can be seen, a pair of symmetrical redox peaks can be found, indicating good reversibility of the electrode. Na_2FePO_4F/C cathodes show two anodic peaks located at about 3.0 V and about 3.7 V corresponding to catholic peaks at about 2.9 V and about 3.6 V at a scan rate of 0.1 mV/s, which are consistent with the two voltage platforms in the charge/discharge curves, respectively. The two pairs of redox peaks probably represent the two reversible phase transformations of $NaLiFePO_4F \longleftrightarrow NaLi_{0.5}FePO_4F$ and $NaLi_{0.5}FePO_4F \longleftrightarrow NaFePO_4F$ based on the mechanism of $NaLiFePO_4F$ electrode reaction [24, 25]. As the scan rate increasing, the anodic peaks move to higher value and the corresponding cathodic peaks move to lower value. But the small potential interval (ΔE_p) between redox peaks (0.29 V for 0.1 mV/s and 0.67 V for 1 mV/s) implies fine reversibility and rate capability [35]. Furthermore, the linear relationship between $v^{1/2}$ and I_p was examined in Figure 6(b), indicating a diffusion controlled process for the electrode reaction. Li^+ diffusion coefficient (D) could be calculated using the Randles-Sevcik equation as:

$$\frac{I_p}{m}=0.4463\left(\frac{F^3}{RT}\right)^{\frac{1}{2}}n^{3/2}AD^{1/2}Cv^{1/2} \quad (1)$$

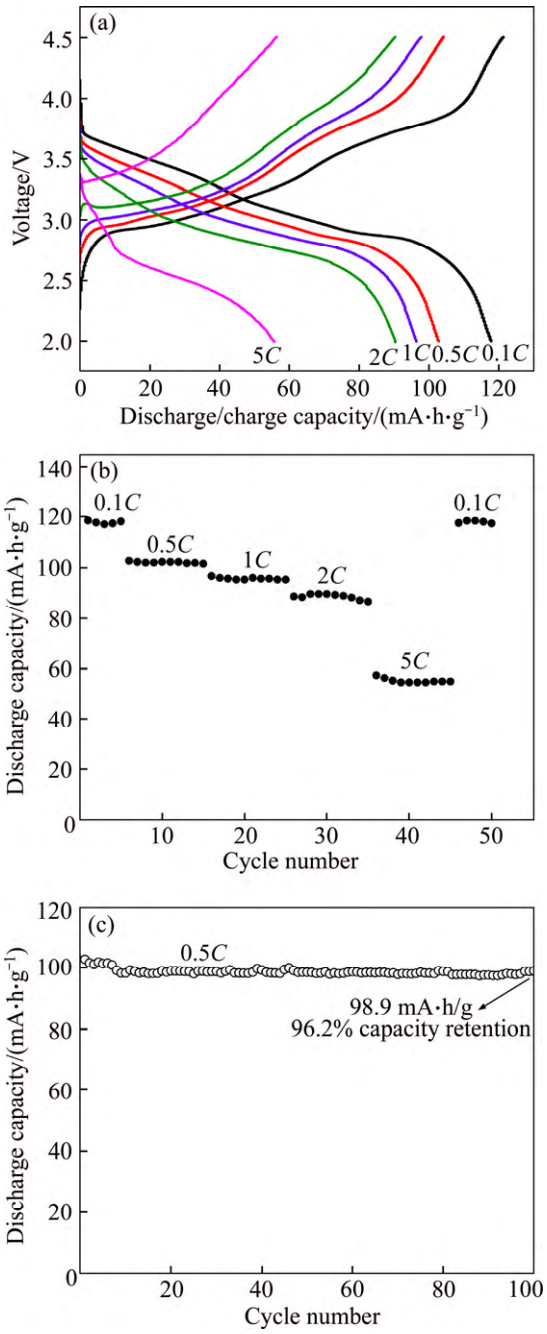

Figure 5 Charge/discharge curves at different rates (a), rate performance (b) and cycling stability cycled at 0.5*C* rate (c) of Na_2FePO_4F/C composite

where m represents the mass of cathode; F is the Faraday constant, R is the general gas constant; T represents the absolute temperature; n is the number of electrons per mole (n=1); A represents the area (A=0.785 m^2); D represents Li^+ diffusion coefficient and C is the Li^+ concentration calculated from the lattice parameters of Na_2FePO_4F. In Figure 6(a), anodic peak (B) and catholic peak (D) fade slowly at a high scan rate (≥0.8 mV/s). The phenomenon is similar to that of the work reported by RUI et al [36]. Thereby, anodic peak (A) and catholic peak (C) might behave as a solid solution behavior, which could be utilized to determine the real Li^+ diffusion coefficient. The calculated values according to anodic peak (B) and catholic peak (D) could be regarded as the apparent result. The Li^+ diffusion coefficients (D) are calculated as follows: 1.40×10^{-9} cm^2/s (peak A), 4.96×10^{-10} cm^2/s (peak B) and 1.71×10^{-9} cm^2/s (peak C), and 3.70×10^{-10} cm^2/s (peak D).

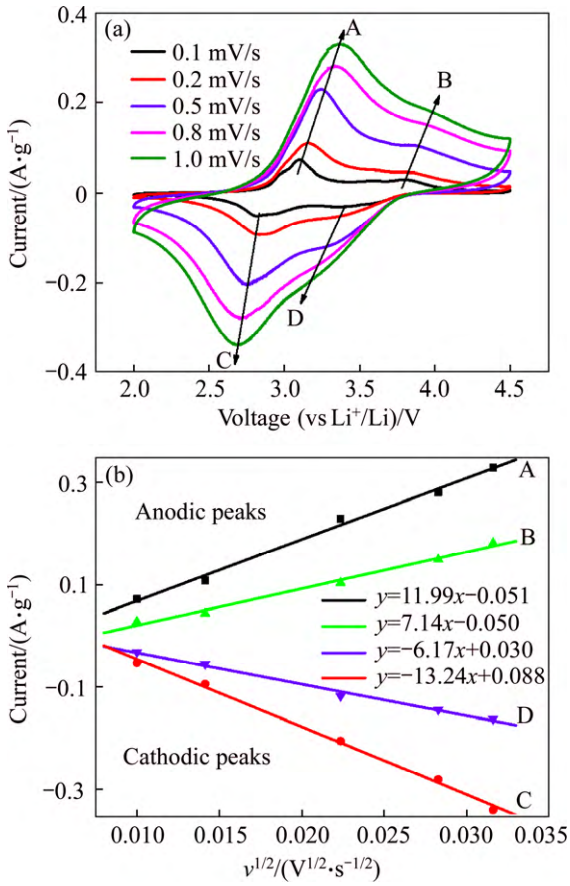

Figure 6 CV curves at different scan rates of Na_2FePO_4F/C in range of 2.0–4.5 V vs Li^+/Li (a) and linear relationship between square root of scan rate $v^{1/2}$ and peak current I_p (b)

EIS is further used to explore the electrochemical performance of Na_2FePO_4F/C composite. The Nyquist plot is given in Figure 7(a). The high-frequency semicircle is ascribed to SEI film resistance, and the semicircle in the middle-frequency is related to the charge transfer resistance. The inclined line at the low frequency is the Warburg impedance (Z_w) which is associated with the Li^+ diffusion into the electrode. Figure 7(b) is the equivalent circuit used to fit EIS. Here, R_e is the solution resistance, R_{sf} is SEI resistance and R_{ct} is

charge transfer resistance. CPE_1 and CPE_2 represent double layer capacitance of solid electrolyte interface (SEI) and the capacitance at the electrode-electrolyte interface, respectively. W_s is the Warburg element. Apparently, the fitting pattern is in good agreement with the experimental EIS data. The fitted impedance parameters are listed in Table 1. As seen in Table 1, R_{ct} and R_{sf} values of Na_2FePO_4F/C electrode are 199.4 and 250.7 Ω, respectively, suggesting that redox reaction of electrolyte/electrode takes place easily.

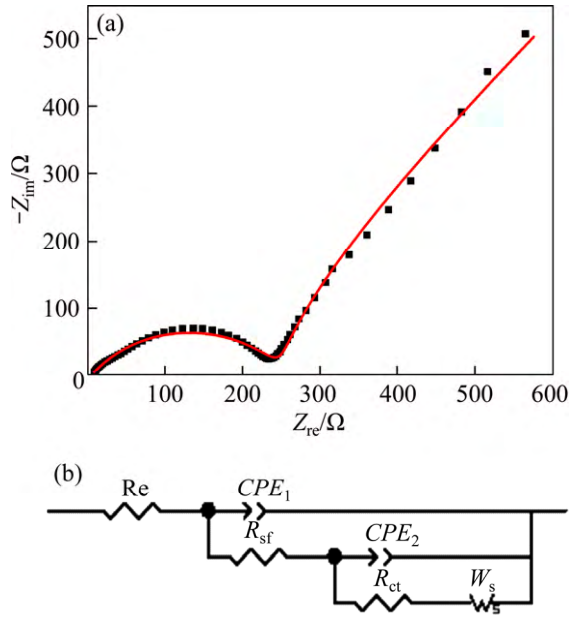

Figure 7 Nyquist plot of Na_2FePO_4F/C electrode (a) and equivalent circuit model (b)

Table 1 Impedance parameters of fitting equivalent circuit

Parameter	Value	Error/%
R_e/Ω	5.359	5.428
CPE_1/F	6.368×10^{-5}	6.418
R_{sf}/Ω	250.7	1.456
CPE_2/F	0.0058	3.59
R_{ct}/Ω	199.4	0.48
W_s/($\Omega^{-1}\cdot cm^{-2}\cdot s^{1/2}$)	0.0028	11.820

4 Conclusions

The Na_2FePO_4F/C composite with uniform particle distribution is prepared by solid state reaction. The EIS result indicates that Na_2FePO_4F/C electrode has small charge-transfer resistance. The Na_2FePO_4F/C composite as cathode materials for LIBs exhibits improved cycling stability and rate performance. It exhibits a discharge capacity of 102.8 mA·h/g at 0.5C, and superior capacity retention of 96.2% after 100 cycles. Discharge capacity of 96.4 mA·h/g at 1C and 90.3 mA·h/g at 2C are achieved. The improved electrochemical performance is ascribed to small size of nanoparticles and uniform carbon-coating. Spherical-like nanostructures lead to the increased interface of electrode/electrolyte and shortened transport distances of both electron and Li^+. Thus, the preparation of Na_2FePO_4F/C composite is an effective method to enhance the performance of Na_2FePO_4F for the application in LIBs.

References

[1] GOODENOUGH J B, PARK K S. The Li-ion rechargeable battery: A perspective [J]. Journal of the American Chemical Society, 2013, 135(4): 1167–1176.

[2] ZHANG Ye, BAI Wen-yu, CHENG Xun-liang, REN Jing, WENG Wei, CHEN Pei-ning, FANG Xin, ZHANG Zhi-tao, PENG Hui-sheng. Flexible and stretchable lithium-ion batteries and supercapacitors based on electrically conducting carbon nanotube fiber springs [J]. Angew Chem Int Ed, 2014, 53: 14564–14568.

[3] DUNN B, KAMATH H, TARASCON J M. Electrical energy storage for the grid: A battery of choices [J]. Science, 2011, 334: 928−935.

[4] LI Wen-liang, NI Er-fu, LI Xin-hai, GUO Hua-jun. Effect of binary conductive additive mixtures on electrochemical performance of polyoxomolybdate as cathode material of lithium ion battery. [J]. Journal of Central South University, 2016, 23: 2506–2512.

[5] LI Hong, WANG Zhao-xiang, CHEN Li-quan, HUANG Xue-jie. Research on advanced materials for Li-ion batteries [J]. Advanced Materials, 2009, 21: 4593–4607.

[6] ANTOLINI E. $LiCoO_2$: Formation, structure, lithium and oxygen nonstoichiometry, electrochemical behaviour and transport properties [J]. Solid State Ionics, 2004, 170(1): 159–171.

[7] LEE M J, LEE S H, OH P, KIM Y S, CHO J. High performance $LiMn_2O_4$ cathode materials grown with epitaxial layered nanostructure for Li-ion batteries [J]. Nano Lett, 2014, 14(2): 993–999.

[8] YANG Jin-li, WANG Jia-jun, TANG Yong-ji, WANG Dong-niu, LI Xi-fei, HU Yu-hai, LI Ru-ying, LIANG Guo-xian, SHAM T K, SUN Xue-liang. $LiFePO_4$-graphene as a superior cathode material for rechargeable lithium batteries: Impact of stacked graphene and unfolded graphene [J]. Energy Environ Sci, 2013, 6: 1521–1528.

[9] HOU Hong-shuai, CRAIG E B, JING Ming-jun, ZHANG Yan, JI Xiao-bo. Carbon quantum dots and their derivative 3D porous carbon frameworks for sodium-ion batteries with ultralong cycle life [J]. Advanced Materials, 2015, 27: 7861–7866.

[10] HOU Hong-shuai, SHAO Li-dong, ZHANG Yan, ZOU Guo-qiang, CHEN Jun, JI Xiao-bo. Energy storage: Large-area carbon nanosheets doped with phosphorus: A high-performance anode material for sodium-ion batteries [J]. Advanced Science, 2017, 4: 1600243.

[11] ZHAO Gang-gang, ZHANG Yang, YANG Li, JIANG Yun-ling, ZHANG Yu, HONG Wan-wan, TIAN Ye, ZHAO Hong-bo, HU Jiu-gang, ZHOU Liang, HOU Hong-shuai, JI Xiao-bo, MAI Li-qiang. Nickel chelate derived NiS_2 decorated with bifunctional carbon: An efficient strategy to promote sodium storage performance [J]. Advanced Functional Materials, 2018, 28: 1803690.

[12] DENG Ming-xiang, LI Si-jie, HONG Wan-wan, JIANG Yun-ling, XU Wei, SHUAI Hong-lei, ZOU Guo-qiang, HUA Yun-chu, HOU Hong-shuai, WANG Wen-lei, JI Xiao-bo. Octahedral Sb_2O_3 as high-performance anode for lithium and sodium storage [J]. Materials Chemistry and Physics, 2019, 223: 46–52.

[13] XUE Xia, SUN Dan, ZENG Xian-guang, HUANG Xiao-bing, ZHANG He-he, TANG You-gen, WANG Hai-yan. Two-step carbon modification of $NaTi_2(PO_4)_3$ with improved sodium storage performance for Na-ion batteries [J]. Journal of Central South University, 2018, 25: 2320–2331.

[14] SHIGETO O, TAKAHASHI Y, KIYABU T, DOI T, YAMAKI J I, NISHIDA T. Layered transition metal oxides as cathodes for sodium secondary battery [J]. ECS Meeting Abstracts, 2006, 602: 201.

[15] YAMADA Y, DOI T, TANAKA I, OKADA S, YAMAKI J I. Liquid-phase synthesis of highly dispersed $NaFeF_3$ particles and their electrochemical properties for sodium-ion batteries [J]. Journal of Power Sources, 2011, 196: 4837–4841.

[16] LIU Yong-chang, ZHANG Ning, WANG Fan-fan, LIU Xiao-bin, JIAO Li-fang, FAN Li-zhen. Approaching the downsizing limit of maricite $NaFePO_4$ toward high-performance cathode for sodium-ion batteries [J]. Adv Funct Mater, 2018, 28: 1801917−1801925.

[17] RECHAM N, CHOTARD J N, DUPONT L, DJELLAB K, ARMAND M, TARASCON J M, Ionothermal synthesis of sodium-based fluorophosphate cathode materials [J]. Journal of the Electrochemical Society, 2009, 156: A993–A999.

[18] ELLIS B L, MAKAHNOUK W R, MAKIMURA Y, TOGHILL K, NAZAR L F. A multifunctional 3.5 V iron-based phosphate cathode for rechargeable batteries [J]. Nature Materials, 2007, 6: 749–753.

[19] ELLIS B L, MAKAHNOUK W R M, ROWAN-WEETALUKTUK W N, RYAN D H, NAZAR L F. Crystal structure and electrochemical properties of A_2MPO_4F fluorophosphates (A=Na, Li; M=Fe, Mn, Co, Ni) [J]. Chemistry of Materials, 2010, 22: 1059–1070.

[20] WU Xiao-biao, ZHENG Jian-ming, GONG Zheng-liang, YANG Yong. Sol-gel synthesis and electrochemical properties of fluorophosphates $Na_2Fe_{1-x}Mn_xPO_4F/C$ (x=0, 0.1, 0.3, 0.7, 1) composite as cathode materials for Lithium ion battery [J]. Journal of Materials Chemistry, 2011, 21: 18630–18637.

[21] ZHOU Jing-jing, ZHOU Jie-feng, TANG Yuan-hao, BI Yu-jing, WANG Chen-yun, WANG De-yu, SHI Si-qi. Synthesis of Na_2FePO_4F/C and its electrochemical performance [J]. Ceramics International, 2013, 39: 5379–5385.

[22] SONG Wei-xin, JI Xiao-bo, WU Zheng-ping, ZHU Yi-rong, YAO Yin-peng, HUANGFU K, CHEN Qi-yuan, BANKS C E. Na_2FePO_4F cathode utilized in hybrid-ion batteries: A mechanistic exploration of ion migration and diffusion capability [J]. Journal of Materials Chemistry A, 2014, 2: 2571.

[23] ELLIS B L, LEE K T, NAZAR L F. Positive electrode materials for Li-ion and Li-batteries [J]. Chemistry of Materials, 2010, 22: 691–714.

[24] BARKER J, SAIDI M Y, SWOYER J L. A sodium-ion cell based on the fluorophosphate compound $NaVPO_4F$ [J]. Electrochemical and Solid-State Letters, 2003, 6: A1–A4.

[25] SONG Wei-xin, LIU Su-qin. A sodium vanadium three-fluorophosphate cathode for rechargeable batteries synthesized by carbothermal reduction [J]. Solid State Sciences, 2013, 15: 1–6.

[26] KAWABE Y, YABUUCHI N, KAJIYAMA M, FUKUHARA N, INAMASU T, OKUYAMA R, NAKAI I, KOMABA S. Synthesis and electrode performance of carbon coated Na_2FePO_4F for rechargeable Na batteries [J]. Electrochemistry Communications, 2011, 13: 1225–1228.

[27] BRISBOIS M, CAES S, SOUGRATI M T, VERTRUYEN B, SCHRIJNEMAKERS A, CLOOTS R, ESHRAGHI N, HERMANN R P, MAHMOUD A, BOSCHINI F. Na_2FePO_4F/multi-walled carbon nanotubes for lithium-ion batteries: Operando Mössbauer study of spray-dried composites [J]. Solar Energy Materials and Solar Cells, 2016, 148: 67–72.

[28] KABALOV Y K, SIMONOV M A, BELOV N V. The crystal structure of sodium iron orthophosphate $Na_2Fe(PO_4)(OH)$ [J]. Doklady Akademii Nauk SSSR, 1974, 215: 850–853.

[29] SWAFFORD S H, HOLT E M. New synthetic approaches to monophosphate fluoride ceramics: Synthesis and structural characterization of $Na_2Mg(PO_4)F$ and $Sr_5(PO_4)_3F$ [J]. Solid State Sciences, 2002, 4: 807–812.

[30] SANZ F, PARADA C, RUIZ-VALERO C. Crystal growth, crystal structure and magnetic properties of disodium cobalt fluorophosphate [J]. Journal of Materials Chemistry, 2001, 11: 208–211.

[31] AVDEEV M, LING C D, TAN T T, LI S, OYAMA G, YAMADA A, BARPANDA P. Magnetic structure and properties of the rechargeable battery insertion compound Na_2FePO_4F [J]. Inorganic Chemistry, 2014, 53: 682–684.

[32] TRIPATHI R, WOOD S M, ISLAM M S, NAZAR L F. Na-ion mobility in layered Na_2FePO_4F and olivine $Na[Fe,Mn]PO_4$ [J]. Energy & Environmental Science, 2013, 6: 2257–2264.

[33] CUI Dong-ming, CHEN Sha-sha, HAN Chang, AI Chang-chun, YUAN Liang-jie. Carbothermal reduction synthesis of carbon coated Na_2FePO_4F for lithium ion batteries [J]. Journal of Power Sources, 2016, 301: 87–92.

[34] BRISBOIS M, KRINS N, HERMANN R P, SCHRIJNEMAKERS A, CLOOTS R, VERTRUYEN B, BOSCHINI F. Spray-drying synthesis of Na_2FePO_4F/carbon powders for lithium-ion batteries [J]. Materials Letters, 2014, 130: 263–266.

[35] SONG Wei-xin, JI Xiao-bo, WU Zheng-ping, ZHU Yi-rong , LI Fang-qian, YAO Yin-peng, BANKS C E. Multifunctional

dual $Na_3V_2(PO_4)_2F_3$ cathode for both lithium-ion and sodium-ion batteries [J]. RSC Advances, 2014, 4: 11375–11383.

[36] RUI X H, DING N, LIU J, LI C, CHEN C H. Analysis of the chemical diffusion coefficient of Lithium ions in $Li_3V_2(PO_4)_3$ cathode material [J]. Electrochimi Acta, 2010, 55: 2384–2390.

(Edited by FANG Jing-hua)

中文导读

简单固相法合成锂离子电池用 Na_2FePO_4F/C 复合材料

摘要：选用二水合磷酸铁为铁源，经乙醇辅助球磨和固相反应制备了氟磷酸亚铁钠/碳复合材料。X-射线衍射证实产品有高的结晶度和相纯度。扫描电镜和透射电镜照片显示，球形氟磷酸亚铁钠粒子的粒径分布在 50~300 nm 之间；从高分辨透射电镜图可以看出，在氟磷酸亚铁钠/碳复合材料的表面包覆了一层厚度为 3.6 nm 的碳层。碳层的包覆能有效地遏制氟磷酸亚铁钠粒子的长大及粒子的团聚。以锂片作为负极组装半电池，在 0.5*C*，1*C*，2*C* 倍率下，复合材料的放电比容量分别为 102.8，96.4，90.3 mA·h/g。0.5*C* 循环 100 次后电池的放电比容量为 98.9 mA·h/g，容量保持率为 96.2%。从循环伏安曲线计算得到氟磷酸亚铁钠/碳复合材料的锂离子扩散系数为 1.71×10^{-9} cm^2/s。显然，固相法是制备锂离子电池正极材料用氟磷酸亚铁钠/C 复合材料的有效方法。

关键词：锂离子电池；氟磷酸亚铁钠/碳复合材料；乙醇辅助球磨；固相反应；球形粒子